CRYSTAL GROWTH & DESIGN

pubs.acs.org/crystal

Article

Ferroelectric Crystals of Globular Molecules: Cambridge Structural Database Mining and Computational Assessment

Elin Dypvik Sødahl,* Seyedmojtaba Seyedraoufi, Carl Henrik Görbitz, and Kristian Berland*

Cite This: *Cryst. Growth Des.* 2023, 23, 8607−8619

Read Online

ACCESS | Metrics & More | Article Recommendations | Supporting Information

ABSTRACT: Hybrid or organic molecular ferroelectrics hold the potential to serve as lead-free alternatives to conventional inorganic ferroelectrics. In particular, the variants composed of globular, often cage-like molecules can host attractive properties such as multiaxial ferroelectricity, Curie temperatures above room temperature, and orientationally disordered plastic mesophases, in addition to supporting low-temperature synthesis. Here, we present the results of a screening study of the Cambridge Structural Database (CSD) leading to the discovery of 54 candidate ferroelectrics, including molecular crystals and molecular salts, many of which are likely to host plastic mesophases, along with 16 previously reported ferroelectrics. With over 1.2 million entries in the CSD, the screening procedure involved many steps, including considerations of molecular geometry and size, space group, and hydrogen bonding pattern. Out of the candidate systems, many of them were identified to be likely to also host plastic mesophases due to their resemblance to highly symmetric close-packed crystal structures. The spontaneous polarization and electronic band gaps were predicted by using density functional theory. Among the candidate ferroelectrics, 17 exhibited a spontaneous polarization greater than 10 $\mu C/cm^2$, with five of them being reported at room temperature.

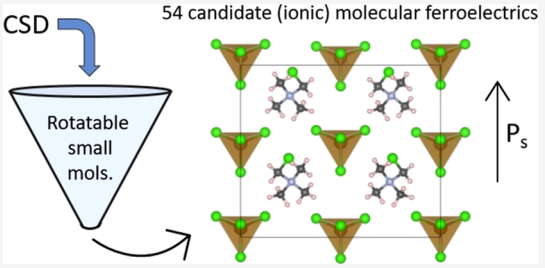

1. INTRODUCTION

Ferroelectric molecular crystals are potential alternatives to conventional inorganic ferroelectrics.[1−4] These materials can be synthesized with low-cost and low-energy methods such as coprecipitation, slow evaporation, spin coating, and 3D printing.[5−11] Furthermore, the abundance of available molecular species allows for tailoring of the properties of molecular crystals while eliminating the need for scarce or toxic elements. The ferroelectric molecular crystals can be formed solely through van der Waals and/or hydrogen bonding, and such systems are referred to as *molecular* crystals. Alternatively, they can also contain an additional ionic component originating from charged molecular species, which are termed *ionic molecular* crystals.

Of particular interest are (ionic) molecular crystals consisting of globular molecules. Their globular shape reduces the steric hindrance of rotational motion, making polarization switching through rotation possible. In some materials, rotational switching can also occur in combination with displacive mechanisms.[12] These materials can show rapid switching with frequencies of up to 263 kHz.[13−15] Moreover, molecular rotations in response to an applied electric field or mechanical force can result in large shear piezoelectric responses.[16] These types of molecular crystals can also crystallize in pseudo high-symmetry structures, thus allowing multiaxial polarization, with as many as 24 equivalent axes.[17−28] Multiaxial polarization allows the spontaneous polarization to be aligned in a desired direction in polycrystalline materials and could allow for multibit storage in single crystals.[29]

Ferroelectric (ionic) molecular crystals, in particular those of globular molecules, can also host orientationally disordered mesophases.[5,28,30−34] These phases can be highly ductile, or "plastic", which can arise from reduced intermolecular interactions, and increased symmetry yielding many facile slip planes.[34] This subgroup of molecular crystals is called plastic crystals, and the materials can be molded and fused, in contrast to the rigidity and brittleness observed for most molecular crystals and inorganic ceramics.[35]

Ferroelectric plastic crystals can exhibit a rich phase diagram,[36,37] with multiple competing crystalline phases and the existence of plastic ferroelectric mesophases. This is exemplified by quinuclidinium perrhenate, which displays a ferroelectric phase with partial orientational disorder.[5] A key advantage of these materials is that they can exhibit low coercive fields. For instance, values in the 2−5 kV/cm range have been reported for compounds such as 1-azabicyclo[2.2.1]heptanium perrhenate and quinuclidinium perrhenate.[5,38] These values are comparable to that of $BaTiO_3$, a well-known inorganic ferroelectric material.[39] Plastic crystals can also exhibit high Curie temperatures, which are

Received: June 12, 2023
Revised: October 28, 2023
Accepted: October 30, 2023
Published: November 14, 2023

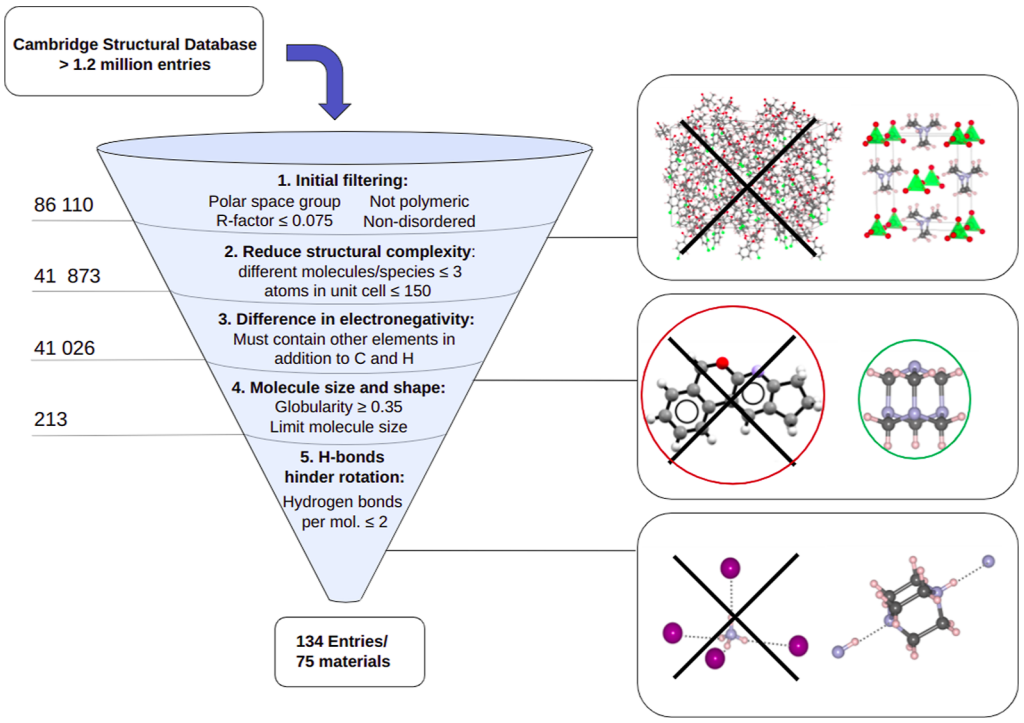

Figure 1. Overview of the screening procedure to identify ferroelectric plastic crystals in the CSD. The numbers on the left indicate the number of structures remaining after each filtering step.

essential for technological applications such as FeRAM and piezoelectric sensing. An example of this is 4-fluoro-1-azabicyclo[2.2.2]octan-1-ium perrhenate which has a Curie temperature of 466 K.[40,41]

In 2020, Horiuchi and Ishibashi compiled a catalog of approximately 80 reported ferroelectric crystals composed of small molecules.[11] This number is very small compared to the collection of approximately 1.2 million organic structures in the Cambridge Structural Database (CSD),[42] which potentially conceals numerous undiscovered ferroelectrics composed of small globular molecules, including plastic crystals. We recently screened this database, leading to the identification of six new candidates for organic proton-transfer ferroelectric materials.[43] In this paper, we provide a comprehensive account of our screening process for molecular ferroelectrics of globular molecules including an assessment of the potential to have plastic mesophases. For all of the systems uncovered, we used density functional theory (DFT) computations for geometry optimization and to predict the spontaneous polarization and the electronic band gaps. These newly identified systems are not only of interest in themselves but also serve as template structures for further crystal engineering, e.g., by substituting molecular species or halides to fine-tune functional properties.

2. METHODS

2.1. Mining the CSD for Ferroelectric Plastic Crystals. To identify candidate ferroelectrics composed in part or fully by small globular molecules, which also could be candidate plastic crystals in the CSD, we employed a systematic filtering process involving five distinct steps, as illustrated in Figure 1.[44] To execute this procedure, we utilized the CSD Python API 3.0.12[42] and the Molcrys[45] package developed by us, based on the Atomic Simulation Environment[46] and Networkx.[47]

Step 1 excluded structures that were nonpolar, polymeric, or disordered, as well as less accurate structures with an *R*-factor ≥0.075.

Step 2 excluded structures with unit cells containing more than 150 atoms. Thus, we avoided time-consuming DFT computations associated with complex and large structures.

Step 3 excluded all material systems composed solely of C and H. This choice was based on the premise that polar covalent bonds or charge transfer between species is needed for high polarization, requiring electronegativity differences.

Step 4 considered the shape of the molecules, removing all structures except those that contained 10 or fewer non-hydrogen atoms, consisted of extended linear segments, or did not contain at least one molecule with a globular or semiglobular geometry. These criteria were motivated by the fact that steric hindrance for molecular rotations should be small in the final structures. The criteria for identifying extended linear segments, such as an aliphatic side group, are detailed in the Supporting Information along with the criteria for globularity.

Step 5 excluded structures where the globular molecules were connected by more than two hydrogen bonds as three directional intermolecular bonds would most likely hinder molecular rotations in all directions.

Following the application of filters, the initial pool of structures was reduced to 75. For each of these, we computed the spontaneous polarization and electronic band gaps using DFT. Note that while we identified a diverse range of systems, the screening criteria have caused some candidates to be omitted. For instance, limiting the number of atoms in the unit cell led to the exclusion of the ferroelectric metal-free plastic perovskite $[NH_3\text{-dabco}]NH_4I_3$ which has 198 atoms in its unit cell. Furthermore, the molecular size constraint excluded some known plastic crystals, including derivatives of adamantane, the C_{60} fullerene,[48−50] and plastic colloidal crystals.[20] However, our primary goal was not to identify all molecular and plastic ferroelectrics but rather to pinpoint several systems of technological interest. Notably, molecular ferroelectrics comprising small molecules typically exhibit a larger density of dipoles, stemming both from individual molecules and intermolecular charge transfer.

2.2. Additional Criteria to Identify Plastic Crystals. While the screening procedure did uncover known plastic crystals, it is likely that many of the candidate systems also have plastic properties. Still, many of the systems would require further investigation to indicate the

https://doi.org/10.1021/acs.cgd.3c00713
Cryst. Growth Des. 2023, 23, 8607−8619

Table 1. Overview of Earlier Reported Plastic Ferroelectrics That Were Discovered in the CSD Screening, Including Curie and Melting Temperatures, T_c and $T_{melt.}$ [K], Coercive Field E_c [kV/cm], Experimental and Computed Spontaneous Polarization, $P_{exp.}$ and $P_{calc.}$ [μC/cm^2], Computed Electronic Bandgap E_g [eV], Crystallographic Space Group, Alignment of Dipoles, and Chemical Composition[a]

CSD refcode	T_c	$T_{melt.}$	E_c	$P_{exp.}$	$P_{calc.}$	E_g	Spg.	alignment (deg)	chem. comp.
				Trimethyl-X-Y					
DIRKEU01[61]	295[61]		67[61]	2.0[61]	5.5	0.3	$Pma2$		$(CH_3)_4N^+$, $FeCl_4^-$
				Cyclic Organic Molecules					
RUJBAC[62]	454[62]			1.1[62]	1.7	1.9	$P2_1$	66, 114; 36	$2C_6H_{12}F_2N^+$, PbI_4^{2-}
BUJQIJ[40]	470[40]		10.8[40]	0.48[40]	2.7	4.6	$P2_1$	76; −	$C_6H_{13}FN^+$, I^-
BUJQOP[40]	470[40]		9.4[40]	0.40[40]	2.8	4.6	$P2_1$	76; −	$C_6H_{13}FN^+$, I^-
				Dabco-Based					
SIWKEP[63]	374[63]		30[63]	9.0[63]	8.0[16]	3.6	Cm		$C_6H_{13}N_2^+$, ReO_4^-
TEDAPC28[64]	378[37]			4[64]	5.9	5.2	$Pm2_1n$		$C_6H_{13}N_2^+$, ClO_4^-
WOLYUR08[65]	374[65]			5[65]	6.2	5.3	$Pm2_1n$		$C_6H_{13}N_2^+$, BF_4^-
BILNES[66]	390[66]				15.9	4.5	$R3r$	52; −	$C_7H_{16}N_2^{2+}$, NH_4^+, $3Br^-$
BILNOC[66]	446[66]		6−12[66]	22[66]	22.4	4.0	$R3r$	52; −	$C_7H_{16}N_2^{2+}$, NH_4^+, $3I^-$
				Quinuclidinium-Based					
LOLHIG02[41]	466[41]			11.4[41]	12.7[16]	4.4	Pn	3; −	$C_7H_{13}FN^+$, ReO_4^-
OROWAV[5]	367[5]		340[5]	5.2[5]	7.3[16]	4.5	$Pmn2_1$	5; −	$C_7H_{14}N^+$, ReO_4^-
YASKIP[17]	322[17]		255[17]	6.7[17]	6.5[16]	2.9	$Pmn2_1$	6; −	$C_7H_{14}N^+$, IO_4^-
SIYWUT[67,68]			1000[68]	1.7[68]	5.6[16]	5.3	$P4_1$	113; −	$C_7H_{14}NO^+$, Cl^-
ABIQOU[68]					5.2[16]	5.0	$P4_1$	113; −	$C_7H_{14}NO^+$, Br^-
MIHTEE[69]	400[69]	492		6.96[69]	10.2	4.6	$P6_1$	85	(R)-$C_7H_{13}NO$
QIVQIY[69]	400[69]			6.72[69]	10.2	4.5	$P6_5$	85	(S)-$C_7H_{13}NO$
				Other Dielectric/Piezoelectric Properties Characterized					
ZZZVPE02[70]		367[34]			17.2	6.4	$R3m$	0	$(CH_3)_3BH_3N$
BOXCUO[71]						0	$P6_3mc$		$(CH_3)_4P^+$, $FeCl_4^-$
QIMXER[72]					9.1	4.7	$Cmc2_1$		$C_6H_{13}N_2^+$, Cl^-
BOBVIY12[73]					6.7	3.8	$Pmc2_1$		$C_6H_{13}N_2^+$, I^-
BOCKEK06[74]					12.2	4.8	$P1$		$C_6H_{13}N_2^+$, HF_2^-

[a]Melting points are retrieved from the CSD unless a reference is listed. The alignment of dipoles is expressed as the angle between molecular dipoles and the polarization axis, as explained in Section 3.3. The lowest temperature structure is listed for refcode families with more than one entry.

existence of a mesophase with plastic ductility. The presence of small globular molecules often allows for a rotational switching mechanism. However, in some systems, the switching path may not be clear-cut, necessitating more complex computations or experimental investigations for full evaluation. Second, for a material to host a plastic mesophase may require not only the existence of an orientationally disordered phase but also that this discorded phase has many facile slip planes, in particular, for the ionic systems. The transition to an orientationally disordered mesophase may involve significant repositioning of the molecules and shifts in the crystal structure, and it is not straightforward to assess the nature of the corresponding disordered phase if such a phase exists. Nonetheless, structures that pack in pseudo close-packed high-symmetry structures are more likely to host a plastic mesophase, as many slip planes would be available with the transition of a high orientational disorder. To assess the similarity to high-symmetry structures, we compared the overlap of radial distribution function (RDF) formed by the center-of-position of each molecule with those of reference structures, representing each molecule/atom as a Gaussian function, $g(r) = \exp[-(r - r_{dist.})^2/2\sigma^2]$, with a small broadening σ to obtain a smooth radial distribution function. The RDFs were scaled so that the first peak positions were set to unity using a Gaussian broadening of $\sigma = 0.1$ for the ionic, and $\sigma = 0.07$ for the molecular crystals, i.e., in units effectively corresponding to the average center-to-center separations of the molecules. The overlap between the RDFs of the template structures and a given molecular crystal was performed with a scaled-distance cutoff of 2.3. The degree of overlap O was evaluated as follows

$$M = \int_0^{r_{cut}} dr\ |\mathrm{RDF}(r) - \mathrm{RDF}^{template}(r)| \quad (1)$$

$$A = \int_0^{r_{cut}} dr\ \mathrm{RDF}(r) \quad (2)$$

$$B = \int_0^{r_{cut}} dr\ \mathrm{RDF}^{template}(r) \quad (3)$$

$$O = [1+M^2/(M - (A + B))^2]^{-1} \quad (4)$$

For the ionic molecular crystals, the overlap was defined as the sum of the overlap for cations and anions combined and the overlap for cations and anions treated separately, i.e., $O = 0.5\ O_{anions,\ cations} + 0.25\ (O_{anions} + O_{cations})$.

In addition to this structure analysis, we also identified materials systems for which an orientationally disordered phase had been reported in the CSD. Since our initial CSD screening excluded disordered structures, all structures within each refcode family were investigated for competing disordered phases. In addition, to identify systems in which the disordered phase had been reported with a different refcode, we performed a structure search using Conquest.[51]

2.3. Density Functional Theory Calculations. The DFT computations were carried out using the VASP software package[52−55] with the projector augmented plane wave method (PAW) pseudopotentials.[56,57] The plane wave cutoff was set to 530 eV for all computations. A Γ-centered Monkhorst−Pack **k**-point grid with a spacing of 1/15 Å^{-1} was used to sample the Brillouin zone. All structures were relaxed until the forces were reduced to below 0.01 eV/Å.

https://doi.org/10.1021/acs.cgd.3c00713
Cryst. Growth Des. 2023, 23, 8607−8619

Table 2. Overview of Candidate Ferroelectric Plastic Crystals That Were Discovered in the Screening of the CSD[a]

	CSD refcode	$T_{struct.}$	$T_{melt.}$	$P_{calc.}$	E_g	Spg.	alignment (deg)	chem. comp
				Trimethyl-X-Y				
M(olecular)	ZZZVPQ01	RT		3.0	5.8	*R3mr*	0	$(CH_3)_3SO_3N$
	LINZOX	RT		6.4	4.4	*Ama2*	63	$(CH_3)_3NH_3Al$
	TMAMBF11	100 (RT)	415[34]	20.3	7.4	*R3m*	0	$(CH_3)_3BF_3N$
	CAVJOZ	193		0.04	2.8	$P6_3mc$		$(CH_3)_3Cl_2Nb$
	TBUHLB05	180	254	7.3	4.9	$Pmn2_1$	19, 32, 33	$(CH_3)_3BrC$
	ETIPAY	160	183	5.5	5.3	$Pna2_1$	20	$(CH_3)_3CH_2ClSi$
I(onic)	WAGGAM	RT		11.0	2.7	$P2_1$	6, 83; –	$2(CH_3)_3OS^+$, $Cr_2O_7^{2-}$
	GEPZIK	123	185	3.9	7.6	$P6_3$		$(CH_3)_3HN^+$, F^-, 6HF
	ZISCUC	300		7.0	0.2	*Cm*	70; –	$(CH_3)_3CH_2ClN^+$, $FeCl_4^-$
	YODGON	RT		3.1	5.0	$Pmn2_1$		$(CH_3)_4N^+$, OCN^-
	VUGNUG	RT		0.12	5.3	$Pmn2_1$		$(CH_3)_4N^+$, N_3^-
	XAKBUG	223		4.5	2.6	*Abm2*	103; –	$(CH_3)_4N^+$, $OsFO_4^-$
	MIWBEC	293		13.4	0.2	$Pca2_1$	53; –	$(CH_3)_4N^+$, $FeCl_3NO^-$
	ORUKUK	100		12.9	3.0	$Pna2_1$		$(CH_3)_4N^+$, $Cl_3F_4^-$
	ZOYGUP	RT	484	3.1	4.1	$P2_1$	68; –	$(CH_3)_4N^+$, $C_5H_7O_4^-$
	SEYLAJ	123	317	12.1	5.2	$P3_1$		$(CH_3)_4N^+$, OH^-, $4H_2O$
	PEVXOE	100			0	$Cmc2_1$		$(CH_3)_4P^+$, O_2^-, $2NH_3$
	PEVXUK	100			0	$Cmc2_1$		$(CH_3)_4As^+$, O_2^-, $2NH_3$
	XENFAZ	295	493	8.4	1.7	$P2_1$	17, 161; –	$2(CH_2O)_3NH_3C^+$, HgI_4^{2-}
				Dabco-Based				
M	LOLWEO	RT	429	7.6	3.4	*Cc*	18, 161; –	$C_6H_{12}N_2$, $2CH_4N_2S$
	HUSRES	150		7.9	4.8	$Pca2_1$	–; 14	$C_6H_{12}N_2$, $C_2H_5O_5P$
I	USAFIG	295		0.4	3.4	$Pna2_1$	95; –	$C_6H_{13}N_2O_2^+$, NO_3^-
	VAGVAA01	150		12.8	5.1	$Pna2_1$		$C_6H_{14}N_2^{2+}$, $2Cl^-$
	GASBIO	123		11.2	4.2	$Pca2_1$		$C_6H_{14}N_2^{2+}$, $2I^-$, H_2O
	NAKNOF03	150		13.4	6.8	*P1*		$C_6H_{14}N_2^{2+}$, $2BF_4^-$, H_2O
				Hexamine-Based				
M	INEYUY/TAZPAD	100 (RT)		0.9	3.8	*R3m*	0	$C_6H_{12}N_3P$
I	HMTAAB	RT		11.6	4.8	$P6_3mc$		$C_6H_{12}N_4$, NH_4^+, BF_4^-
	BOHNUH01	295		10.6	4.9	*R3m*	83; –	$C_6H_{13}N_4^+$, Br^-
	TOZTAF	296		17.3	4.3	*Cc*	138; 89	$C_6H_{13}N_4^+$, $C_4H_5O_5^-$
				Boron Clusters				
M	SASSOU	RT	378	7.7	3.5	*Cc*	80	$CH_{10}B_6S_2$
	OTOLAM	150		11.5	5.5	*Pnn2*	0	$C_2H_{14}B_8$
I	UTUZAM	90		3.2	4.8	$P2_1$	56; –	$CH_{14}B_9^-$, $C_3H_{10}N^+$
	LUWHOD	340		7.8	4.4	$P4_2$		$B_{10}H_{10}^{2-}$, $2NH_4^+$, NH_3
				Cyclic Organic Molecules				
I	WAQBOH	295		8.1	5.7	*Pn*		$C_4H_{11}N_2^+$, BF_4^-
	CUWZOM	100		0.4	5.5	$P2_1$	52; –	$C_5H_{11}FN^+$, Cl^-
	AMINIT	293		6.8	4.5	$P2_1$	126; 88	$C_5H_{12}N^+$, $H_2AsO_4^-$
	EVULAI	100		13.2	4.7	$P2_1$	39	$C_6H_{15}N_2S^+$, Cl^-
	FENYEC	RT	407	4.9	3.5	*Cc*	55; 85	$C_7H_5O_3^-$, $C_4H_{10}N^+$
	HAJXEW	123		16.5	5.6	*Pn*	16; –	$C_6H_{18}N_3^{3+}$, ClO_4^-, $2Cl^-$
	OBEXEY	200	416	7.6	4.8	$Cmc2_1$		$C_9H_{20}N^+$, N_3^-
				Cage-like Organic Molecules				
M	EQAXOL	140		9.1	5.4	$Pna2_1$	48	$C_5H_9O_3P$
	BAPFAB	150		4.1	5.3	$P2_1$	20, 56	$C_6H_7FO_3$
	BAPFOP	150		0.7	5.4	$P2_1$	20	$C_6H_7FO_3$
	NOCPIE01	100 (RT)		14.9	4.5	$P2_1$	51, 63	$C_7H_{10}O_3$
	MIRHUQ	180	388 (sublim.)	11.3	4.6	$P2_1$	29, 31	$C_8H_{15}PS$
	XIBVIN	180	443	1.3	4.2	*C2*	77	$C_8H_{15}PS$
	BESWON	130		4.5	5.7	$P3_1$	70	$C_9H_{16}O$
	FEJFAB	RT		7.4	2.1	$Pmc2_1$	34; –	$C_6H_{10}N_2$, CBr_4
I	PINRAI	173		5.3	5.8	$Pna2_1$	60; –	$C_6H_9F_3N^+$, Cl^-
	QAZFUV	100		11.5	5.2	$Cmc2_1$	54; –	$C_6H_{12}N^+$, Cl^-
	JEBVOC	293	>533	8.2	4.4	$P2_1$	70; –	$C_9H_{14}N^+$, Cl^-
				Other				
I	HUPTUI	100		0.4	3.7	$P2_1$	86; –	$C_6H_{18}N_3S^+$, TaF_6^-
	VAJKUM	RT	513	1.7	3.2	$P2_1$	85; 43	$C_6H_{18}N_3S^+$, SF_5O^-
	OTIJUZ	123	393[75]	2.6	5.1	*Pc*	43, 120; –	$2C_6H_{18}OPSi^+$, $S_2O_7^{2-}$

https://doi.org/10.1021/acs.cgd.3c00713
Cryst. Growth Des. 2023, 23, 8607−8619

Table 2. continued

[a]Values have been listed for the melting temperatures $T_{melt.}$ [K], computed spontaneous polarization $P_{calc.}$ [μC/cm^2], computed electronic bandgap E_g [eV], crystallographic space group, alignment of dipoles, and chemical composition. Melting points are retrieved from the CSD unless a reference is listed. $T_{struct.}$ is the temperature at which the structure was determined (RT) and indicates that the structure is also reported at room temperature. The alignment of dipoles is expressed as the angle between molecular dipoles and the polarization axis, as explained in Section 3.3. The lowest temperature structure is listed for refcode families with more than one entry.

The spontaneous polarization was computed using the Berry phase method.[58,59] Rather than identifying nonpolar reference structures, which is the conventional procedure, we gradually increased the spacing between slabs of materials. In this case, the appropriate polarization branch can be identified by a nondiverging dipole element dipole per slab. The supercell size, i.e., the slab thickness, was converged to obtain a reliable description of the dipole moments.

For both relaxation and polarization calculations, the vdW-DF-cx functional was employed,[60] based on the accurate lattice constants determined in our earlier benchmarking study of exchange−correlation functionals for ferroelectric plastic crystals.[16]

3. RESULTS AND DISCUSSION

Among the 75 systems identified through the screening of the CSD, 16 have previously been reported to have ferroelectric properties.[5,17,37,40,41,61−69] Five more have been studied for their piezoelectric and/or dielectric properties but have not explicitly been reported as ferroelectric (CSD refcodes: ZZZVPE02, BOXCUO, QIMXER, BOBVIY12, and BOCKEK06).[70−74] Table 1 provides a summary of the available experimental results along with the computed values for spontaneous polarization and electronic band gaps for both the earlier reported ferroelectric and dielectric/piezoelectric materials. Table 2 lists the computed values for the other systems found in the screening. For three of these systems, the DFT computations did not yield a finite band gap. For these systems, we also computed the band gaps at the HSE06 hybrid functional level by Heyd, Scuseria, and Ernzerhof[76] which also showed an absence of a band gap.

Figure 2 shows an overview of the molecular and ionic molecular crystals among the previously reported and candidate ferroelectrics.

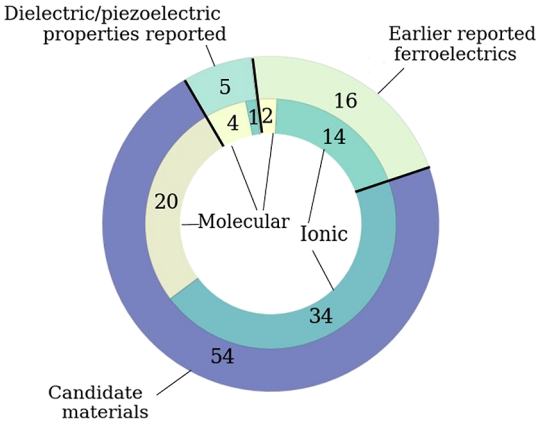

Figure 2. Overview of the candidate ferroelectrics, reported ferroelectrics, and materials with reported dielectric/piezoelectric properties identified in the screening. The outer circle indicates the number of structures in each of these groups, and the inner circle indicates the number of molecular and ionic molecular crystals.

Among the 16 known ferroelectrics, 14 are ionic molecular crystals. For the candidate systems, 20 are classified as molecular, while 35 are ionic molecular crystals.

Figure 3 illustrates a selection of the molecular entities found in these identified systems, which include globular molecules, neutral and charged molecules, and ions. In total, the systems encompass 30 different anionic molecules, 31 cations, and 25 neutral molecules.

Figure 4 outlines the seven distinct groups of systems identified based on the composition and geometry of the globular molecules. Three candidate systems do not fit into any of these categories and are listed as "Other" in Table 2.

Figure 5 compares the computed spontaneous polarization values with experimentally measured values for the previously reported ferroelectric molecular crystals.[5,17,40,41,61−66,68,69] While slightly larger, the computed values overall agree well with the experimental. The larger computed values can be attributed to extrinsic factors such as defects, grain orientation and boundaries, and electronic leakage which can reduce the experimental spontaneous polarization.[77,78] Additionally, atomic vibration and molecular librations may also cause spontaneous polarization to be reduced at a finite temperature. Moreover, the structures used for assessment with DFT were the ones in the CSD determined at the lowest temperature, while remaining the same polymorphs identified in the screening.

3.1. Candidate Ferroelectric Plastic Crystals. *3.1.1. Trimethyl-X-Y Systems.* One group of (ionic) molecular crystals identified in our screening is characterized by the presence of trimethyl-X-Y building blocks, where X denotes an atom and Y a chemical group or atom, as exemplified by the two structures in Figure 4. Among the 22 systems, only one, DIRKEU01, has previously been reported as ferroelectric. ZZZVPE02 has been reported to have a piezoelectric coefficient d_{33} in the range of 10−16 pC/N and a pyroelectric coefficient of ≈25.8 μC/m^2 K.[70] Another compound, BOXCUO has been reported to have switchable dielectric and magnetic properties,[71] but this is one of the compounds for which DFT indicated a lack of electronic band gap.

Among the 19 remaining systems identified, seven are composed of neutral molecules, while the rest are formed from various combinations of 12 different anions and seven different cations. Tetramethylammonium is the most common cation, found in eight out of the 22 systems. The many possible combinations of molecules, and the fact that six of the systems exhibit computed spontaneous polarization values exceeding 10 μC/cm^2 (Table 2), indicate that the trimethyl-X-Y systems hold significant promise. The highest value is found for TMAMBF11 at 20.3 μC/cm^2.

3.1.2. Dabco-Based Systems. Crystals composed of various derivatives of 1,4-diazabicyclo[2.2.2]octane (dabco) in combinations with anions such as ClO_4^- and ReO_4^- have been found to have found to exhibit properties such as low coercive fields and rapid ferroelectric switching with frequencies up to 263 kHz.[13,15,24,63,79] Li et al. reported a Curie temperatures as high as 540 K for *N*-fluoroethyl-*N*-ZnI_3-1,4diazabicyclo[2.2.2]octonium.[80]

In our screening, we identified 13 dabco-based systems, out of which five have previously been reported as ferroelectrics.[37,63−66] Two of these, BILNES and BILNOC, can be classified as organic metal-free perovskites,[66] Figure 4. In addition to the reports of ferroelectric properties, the dielectric response of QIMXER, BOBVIY12, and BOCKEK06 have been characterized by Szafrański et al.[72−74] For the five previously identified ferroelectrics, we computed spontaneous polarization values ranging from 5.9 for TEDAPC28 to 22.4 μC/cm^2 for BILNOC, which can be compared to 0.4−13.4 μC/cm^2 for the additional systems identified. Interestingly, two of them, LOLWEO and HUSRES, are not ionic, but cocrystals of charge-neutral molecules.

3.1.3. Quinuclidinium-Based Systems. Several systems containing variations of the quinuclidinium molecule have been studied in recent years.[6,18,21,28,67−69,81,82] Notably, Tang et al. reported a Curie temperature of 466 K for [F-$C_7H_{13}N$]ReO_4.[41] Another material of interest is $[C_7H_{14}N]IO_4$, for which You et al. found 12 equivalent directions of polarization.[17] The reported coercive fields of these

https://doi.org/10.1021/acs.cgd.3c00713
Cryst. Growth Des. 2023, 23, 8607−8619

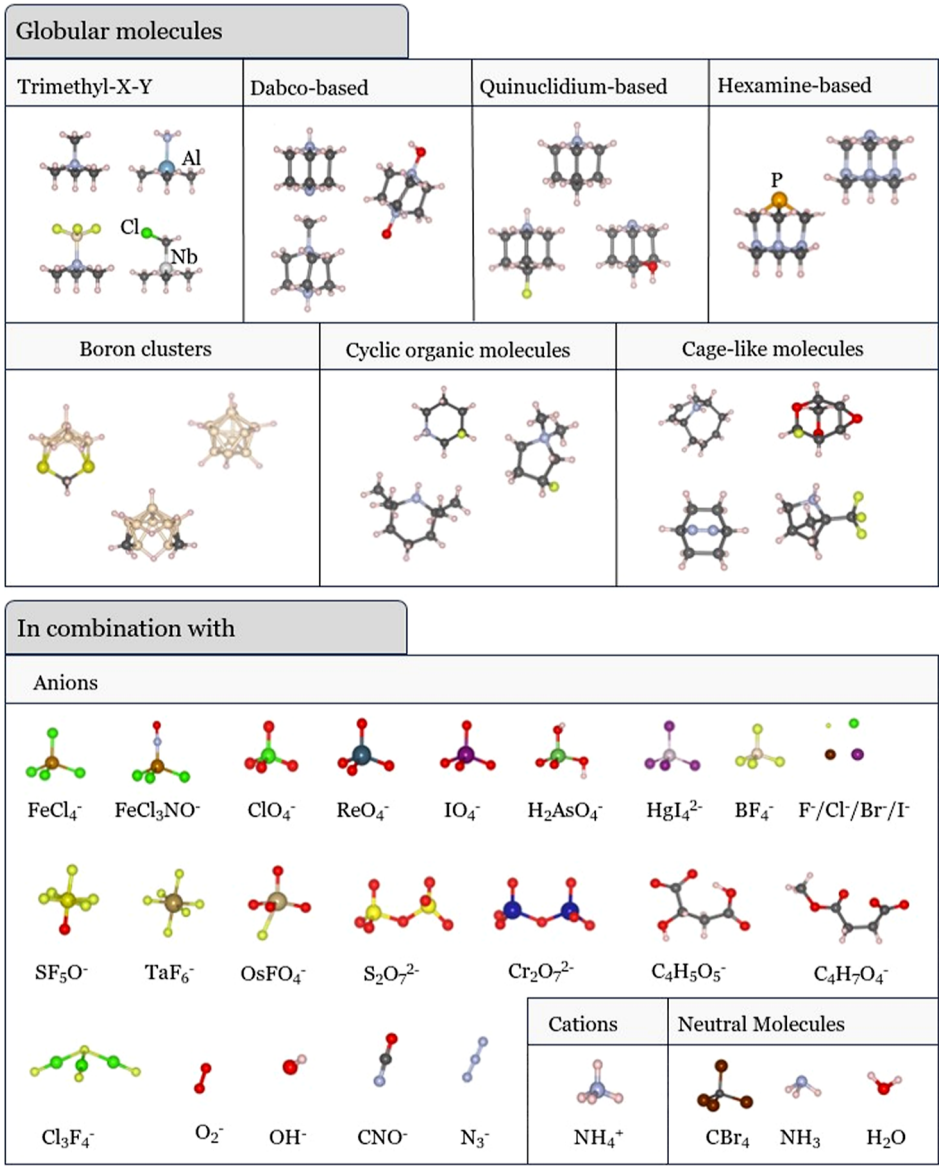

Figure 3. Examples of globular molecules and the anions, cations, and neutral molecules that are combined in the identified structures. In the top panel, carbon atoms are shown in gray, nitrogen in blue, oxygen in red, fluorine in yellow, boron in beige, and hydrogens as white. Other elements are labeled.

compounds are rather high, ranging from 255 to 1000 kV/cm.[68] All seven quinuclidinium-based systems found in this study have previously been reported as ferroelectrics[5,17,38,41,67−69] (Table 1). Five are plastic ionic crystals, while the two remaining are plastic molecular crystals and stereoisomers with identical compositions. The computed spontaneous polarizations of the quinuclidinium systems range from 5.2 to 12.7 μC/cm^2.

3.1.4. Hexamine-Based Systems. In our screening, we identified four hexamine-based crystal structures, none of which, to the best of our knowledge, have been reported as ferroelectrics in the past. Figure 3 shows the two variations of the hexamine molecule that we found, the regular hexamine molecule, and a derivative where a nitrogen atom has been substituted by phosphorus. Three structures are ionic molecular crystals with spontaneous polarizations ranging from 10.6 to 17.3 μC/cm^2 (Table 2). One of these, HMTAAB, features a perovskite-like structure; see Figure 4. The nonionic molecular crystal with a spontaneous polarization of 0.9 μC/cm^2 occurs with two different refcodes in the CSD; TAZPAD and INEYUY. The large spontaneous polarization values of the ionic hexamine-based systems should encourage further experimental characterization and optimization of these types of systems.

3.1.5. Boron Cluster Systems. While boron clusters have been extensively studied for their characteristic chemistry, biological application, and magnetic, optical, and electronic properties,[83−86] their ferroelectric characteristics have not received particular attention. Our screening study identified four systems containing boron clusters (Table 2). Two of them, SASSOU and LUWHOD, were measured at room temperature or higher and have spontaneous polarizations just below 8 μC/cm^2. The highest spontaneous polarization value is computed for OTOLAM, at 11.5 μC/cm^2. The combination of large polarization and room temperature stability renders the boron cluster-based systems interesting for further investigations.

3.1.6. Systems Containing Cyclic Organic Molecules. Ten of the systems identified contain cyclic organic molecules, both aromatic and nonaromatic, and we chose to group these together. All ten are ionic molecular crystals, including three earlier reported ferroelectrics[40,62] (Table 1), two of them have the same composition and are stereoisomers. The third, RUJBAC, is an organic−inorganic hybrid perovskite.[62] All three have spontaneous polarization below 3 μC/cm^2, coercive fields around 10 kV/cm,[40] and exhibit Curie temperatures exceeding 450 K.[40,62] Among the seven candidates

https://doi.org/10.1021/acs.cgd.3c00713
Cryst. Growth Des. 2023, 23, 8607−8619

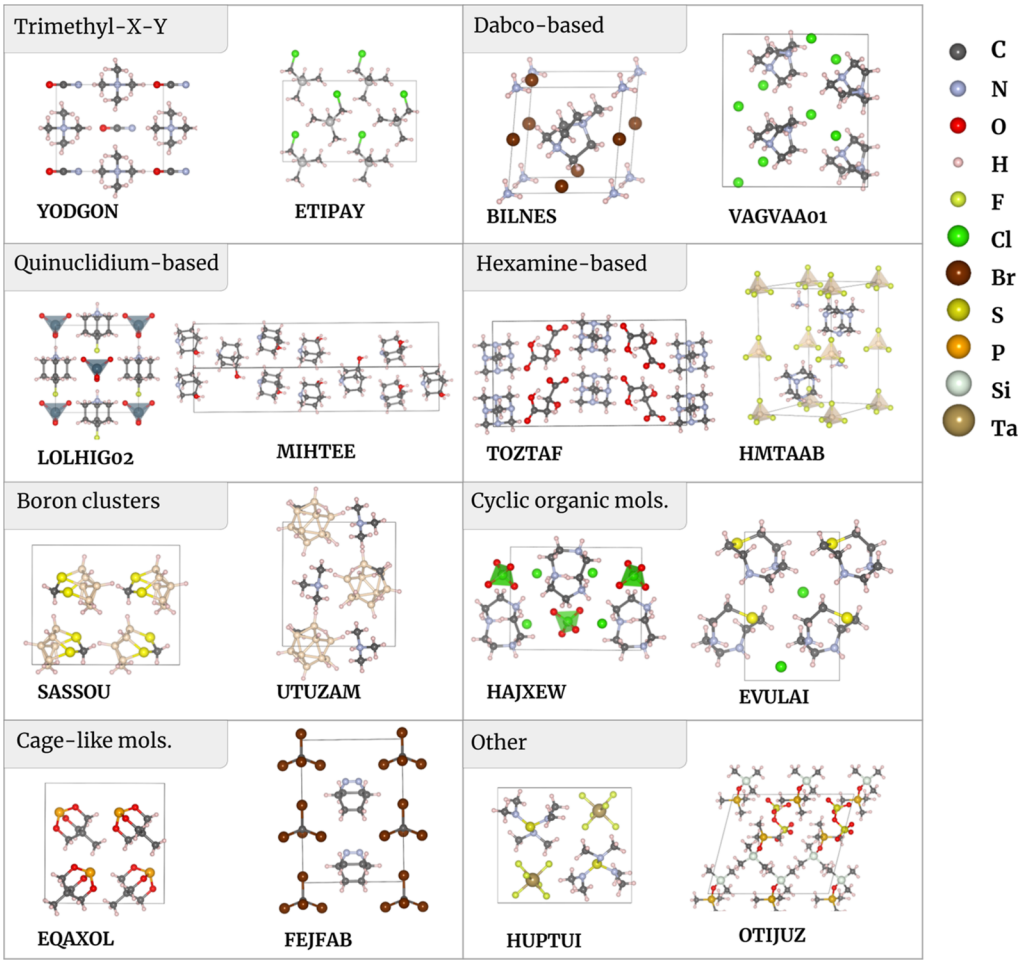

Figure 4. Examples of structures found in each of the eight groups of systems. ETIPAY, MIHTEE, SASSOU, EQAXOL, and FEJFAB are molecular crystals; the remaining are ionic.

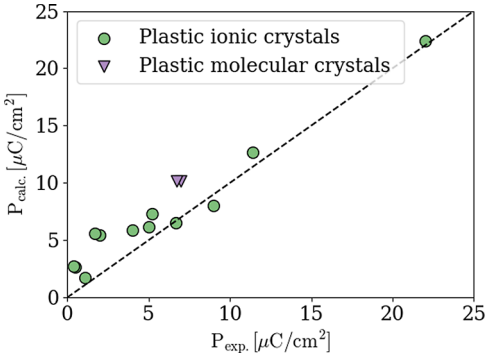

Figure 5. Computed spontaneous polarization compared to the experimentally measured values. Spontaneous polarization is reported for 14 out of the 16 known ferroelectrics identified in the screening.

identified here, all but one have spontaneous polarizations exceeding those of earlier reported ferroelectrics. HAJXEW has the largest value of 16.5 μC/cm^2 (Table 2). Three of the candidates identified, WAQBOH, AMINIT, and FENYEC have been reported as stable at room temperature, with the latter melting above 400 K.

3.1.7. Systems Based on Organic Cage-like Molecules. We found 11 crystal structures containing organic cage-like molecules, none of which have previously been reported as ferroelectric. Seven of these are molecular crystals, while four are ionic (Table 2). Even though there are no reported room temperature structures for MIRHUQ and XIBVIN, their reported sublimation and melting temperatures are high: 388 and 443 K, respectively. JEBVOC is reported to have a melting temperature of exceeding 533 K.

Finally, three of the candidate ferroelectrics do not fit into any of the defined groups. HUPTUI and VAJKUM have similar crystal structures and are built up of tris(dimethylamino)sulfonium molecule and an octahedral inorganic anion. For these systems, the computed spontaneous polarizations are below 3 μC/cm^2.

3.2. Comparison of Candidate and Previously Reported Ferroelectrics. The previously reported ferroelectrics frequently contain cage-like organic molecules, such as dabco and quinuclidinium derivatives, combined with halogen, $FeCl_4^-$, or XO_4^- anions. The molecules in the identified candidates are by comparison generally smaller: 25 systems consist of molecules with five or fewer carbon atoms (not counting structures of boron clusters). The smaller volume of the asymmetric unit allows for larger spontaneous polarization. The lower molecular weights of the smaller molecules of the candidate systems could, however, lead to reduced melting points. Overall, the candidates display a more diverse set of anions that include entities such as HF_2^-, CNO^-, $FeCl_3NO^-$, and SF_5O^-.

3.3. Polarization and Alignment of Molecules. Molecules in plastic crystals often pack in complex arrangements, and the direction of the individual molecular dipoles does not necessarily align with the direction of the spontaneous polarization.[16] In Tables 1 and 2, the "dipolar" direction relative to the polarization direction is listed. Often, the unit cell holds several equivalent molecules that align at the same angle with the polarization axis, as given by space group symmetry. Mirror or rotational symmetries cause the polarization contributions perpendicular to the polarization axis to cancel out. For many of the molecules, their dipolar direction is thus evident from their symmetry, but not all molecules have a clear dipole direction due

https://doi.org/10.1021/acs.cgd.3c00713
Cryst. Growth Des. 2023, 23, 8607−8619

to their low symmetry, and even for symmetric molecules, the direction with respect to the high symmetry direction is not always clear-cut. For these molecules, we obtain an effective "dipole" direction from the moments of the electronegativity relative to the center of electronegativity and compute its relative angle to the overall spontaneous polarization direction.

Figure 6 illustrates the alignment of the molecular dipoles relative to the polarization axis for MIWBEC. In the cases where the molecules are symmetrical or have a negligible dipole, no alignment is listed. In these systems, interspecies charge transfer is the dominant contribution to spontaneous polarization. Examples of such systems are six of the dabco-based systems, SIWKEP, TEDAPC28, WOLYUR08, VAGVAA01, GASBIO, and NAKNOF03. Despite negligible molecular dipoles, their spontaneous polarizations are in the range 5.0−18.4 μC/cm^2. For systems where the molecular dipoles run counter to the overall polarization, an interesting prospect opens up for realignment of the dipoles by application of an electric field. This could both increase the spontaneous polarization and allow for multibit storage, assuming that the electric field required to realign the dipoles is smaller than the coercive field of the ferroelectric material.

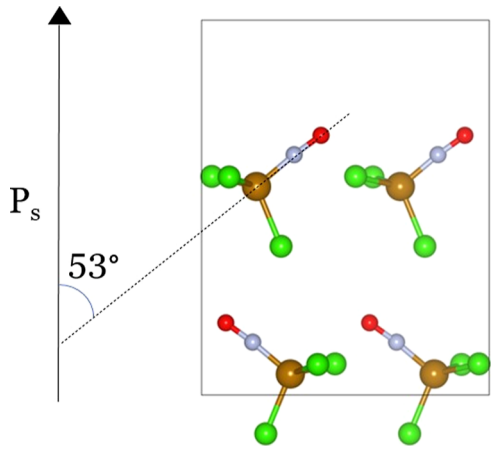

Figure 6. Illustration of the alignment of dipoles in MIWBEC (tetramethylamine molecules omitted for simplicity). The dipoles align along two directions, both 53°, on the polarization axis.

3.4. Plastic Properties of the Candidate Ferroelectrics. While the screening study can identify candidate ferroelectric plastic crystals, truly predicting whether the systems can transition to a plastic mesophase demands more involved simulations, such as molecular dynamics. This is not feasible for the large pool of candidate systems identified in this study, but out of the 16 identified known ferroelectrics, eight are reported to be plastic crystals, namely ABIQOU, SIYWUT, MIHTEE, QIVQIY, DIRKEU01, OROWAV, YASKIP, and LOLHIG02.[5,17,24,61,68,69] WOLYUR08, TEDAPC28, and SIWKEP are reported to have rotationally disordered high-temperature phases, but their mesophase ductility has not been investigated. Furthermore, the high-temperature phases of BUJQIJ and BUJQOP have not been resolved due to poor XRD data,[40] which can indicate the high degree of disorder characteristic for plastic crystals. Three candidate systems have been reported to be plastic crystals where all molecules exhibit rotational disorder, namely TMAMBF11,[34] ZZZVPE02,[34] and ZISCUC.[87] LOLWEO has a reported high-temperature phase in which one of the two molecular constituents shows an orientational disorder. Thus, the screening procedure is suited to identify systems with orientationally disordered mesophases.

High ductility is often linked to the existence of many slip systems. Thus, plastic properties are more likely in an orientationally disordered mesophase with a dense packing and high symmetry. High symmetry is particularly acute for the ionically bonded molecular crystals due to their limited number of slip planes. Thus, ionic molecular crystals that are pseudosymmetric to structures such as CsCl and NaCl are more likely to exhibit plastic behavior.

Figure 7 plots the overlap of the RDFs as defined in eqs 1−4 of systems composed of two molecular entities identified here with the structures of CsCl, NaCl, as well as zincblende. The horizontal line marks the known plastic crystal with the smallest overlap with a reference close-packed structure, namely, ZISCUC with an overlap of 0.83 with the CsCl structure. Structures with a larger overlap are likely to host plastic mesophases. In total, 17 of the systems fulfill these criteria, including all 7 of the materials with previously reported plastic properties. However, it is important to keep in mind that our assessment is quite rough and does not take into account factors such as the available space for rotation; moreover, several of the

Figure 7. Overlap between the ionic molecular crystals identified in the screening with structure types that can allow for plastic properties. The horizontal line marks the lowest overlap calculated for the known plastic crystals identified here. Structures earlier reported as plastic crystals are marked with boldface.

https://doi.org/10.1021/acs.cgd.3c00713
Cryst. Growth Des. 2023, 23, 8607−8619

compounds not fulfilling this criterion may, for instance, exhibit a significant positional shift in the transition to an orientationally disordered mesophase.

Figure 8 plots the overlap between the molecular crystals and hexagonal close-packed (hcp), body-centered cubic (bcc), and face-centered cubic (fcc) structures. Here, the smallest overlap between a known plastic crystal and a reference structure is ZZZVPE02, which has an overlap of 0.96 with the bcc structure and 0.86 with the hcp structure. The close-packed structures built up of a single molecular species are harder to differentiate than the ones composed of two species using the overlap based on the RDF-overlap.

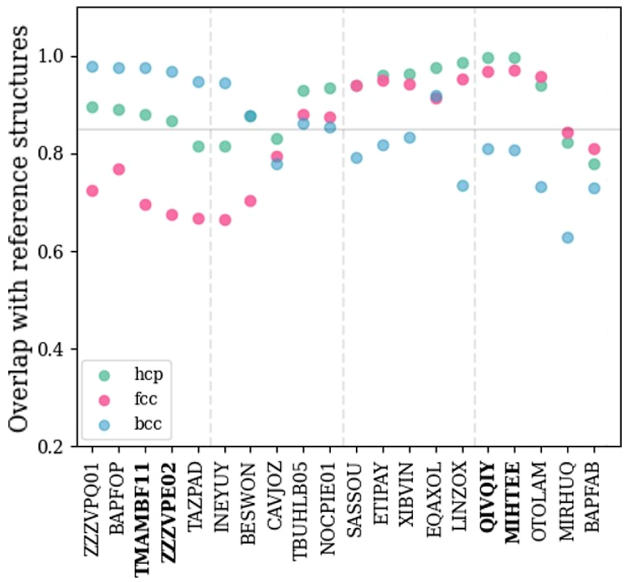

Figure 8. Overlap between the molecular crystals identified in the screening with structure types that can allow for plastic properties. The horizontal line marks the lowest overlap calculated for the known molecular plastic crystals identified here. Structures earlier reported as plastic crystals are marked with boldface.

This is the case for two of the crystals with reported plastic properties, TMAMBF11 and ZZZVPE02, which show large similarities to both hcp- and bcc-type packing. These two isostructural systems crystallize in the *R*3*m* space group, Figure 9, and are reported to have ductility comparable with metals in their plastic phases.[34] A large overlap with the close-packed hcp and fcc structures can indicate plasticity; 14 of the molecular crystals have an overlap larger than 0.86 with the hcp or fcc structures, indicative of plastic properties, including the four reported plastic crystals. Finally, we note that the existence of many slip planes and high symmetry might be less critical for the (nonionic) molecular crystals. Other deformation mechanisms can also be present, such as creep close to the melting temperature. Onset of configurational disorder has been associated with increased plasticity in molecular crystals.

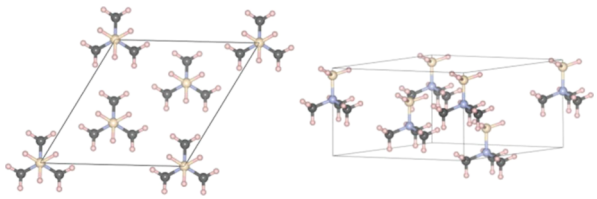

Figure 9. Crystal structure of the plastic molecular crystal ZZZVPE02, isostructural to TMAMBF11.

Overlap with close-packed structures was not evaluated for the 11 structures composed of three molecular entities identified in this study due to their complexity. Out of these, four have perovskite-type structures; RUJBAC, BILNES, BILNOC, and HMTAAB. While these might be less likely to host a plastic mesophase, plastic behavior has earlier been reported for hybrid perovskites.[88−90]

3.5. Thermal Stability. For device applications, thermal stability is an important property and operational temperatures should be significantly below melting and sublimation temperatures. The melting temperature of plastic crystals can be higher than for similar ionic and molecular crystals, due to the high entropy associated with the orientational disorder and increased freedom of movement making melting less favorable, as first reported by Timmermans.[30] The volume change at the phase transition is also small.[91]

For 45 of the 75 systems identified in this study, the crystal structure is ordered with a ferroelectric space group and obtained at ambient temperature. For the four systems, a paraelectric phase is reported at room temperature. Finally, 26 systems lack a reported crystalline room temperature phase in the CSD. The fraction of room temperature investigations is highest for ionic crystals, Figure 10, a result that is in line with the higher stability of the ionic molecular crystals, due to electrostatic interactions.

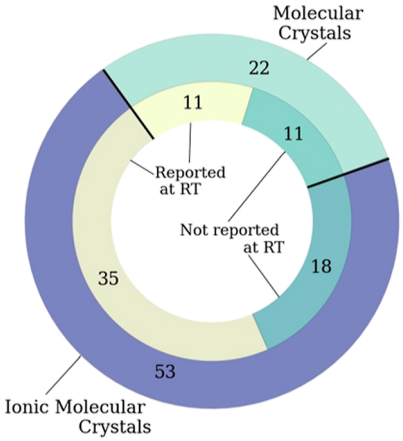

Figure 10. Overview of the molecular and ionic crystals identified. The outer ring indicates the number of systems, and the inner ring indicates if the potentially ferroelectric phase is reported at room temperature.

3.6. Electronic Band Gap and Multisource Energy Harvesting. Ferroelectric materials with band gaps in the visible range can be of particular interest, as these could be promising for application in multisource energy harvesting devices where piezo- or pyroelectric energy harvesting is combined with the harvesting of solar energy.[92,93] Therefore, we computed the band gaps for all identified systems to find those that could be suitable for such applications.

Tables 1 and 2 list the computed band gaps. Since the computations were performed using the vdW-DF-cx functional, which describes exchange at the generalized-gradient approximation level,[60] we can expect the band gaps to be underestimated. Most of the computed band gaps exceed 4 eV; however, six systems have values smaller than 2 eV. Four of these belong to the trimethyl-X-Y group, which could thus be interesting for multisource energy harvesting.

3.7. Design Strategies for Ferroelectric Plastic Crystals. Novel and improved ferroelectric plastic crystals can be engineered by making new combinations of molecular species. As such, the various species found in the various plastic crystal candidates can be used as building blocks for novel material design; a selection of these is displayed in Figure 3.

Of particular interest are substitutions that are likely to result in similar or isostructural crystals. For systems where this is possible, solid-solution engineering can be used to tweak the material properties. Three examples of pairs of candidates for such alterations are found among the trimethyl-X-Y systems. The compositions

https://doi.org/10.1021/acs.cgd.3c00713
Cryst. Growth Des. 2023, 23, 8607−8619

between each pair of systems are similar, only differing by the substitution of molecules with similar geometries. PEVXOE and PEVXUK are isostructural and only differ by the substitution of $(CH_3)_4P^+$ for $(CH_3)_4As^+$. For ZZZVPE02 and TMAMBF11, the substitution of $(CH_3)_3BH_3N$ to $(CH_3)_3BF_3N$ yields an isostructural material where the computed polarization is increased from 17.2 to 20.3 $\mu C/cm^2$. A similar effect is seen for YODGON and VUGNUG, where the substitution of N_3^- for OCN^- leads to an increase in the spontaneous polarization from 0.13 to 3.1 $\mu C/cm^2$.

Another example of substitution resulting in similar packing is the earlier reported ferroelectrics TEDAPC28 and SIWKEP, which consist of a dabco molecule and a tetrahedral inorganic ion, ClO_4^- or ReO_4^-, respectively. This substitution somewhat changes the orientation of molecules, resulting in a different space group. Whereas, we found a spontaneous polarization of 8 $\mu C/cm^2$ for the ReO_4^- system, the ClO_4^- one has a value of 5.9 $\mu C/cm^2$.

In total, ten different tetrahedral inorganic anions were found in our screening study, such as BF_4^-, $FeCl_3ON^-$ and IO_4^-, but other options also exist and can be considered for the design of new ferroelectric plastic crystals. Substitutions of single atoms in the organic globular molecule can also be a route to engineer the ferroelectric properties.[94] For instance, Lin et al. substituted a hydrogen atom in tetramethylammonium for halogens I, Cl, and Br. The crystal structure was retained, while the number of ferroelectric polar axes increased from 2 for iodine to 6 for chlorine.[95]

4. CONCLUSIONS

Using a CSD-based workflow, we identified 54 candidate ferroelectric molecular crystals. The 17 with spontaneous polarization exceeding 10 $\mu C/cm^2$ are arguably the ones with the most potential in ferroelectric devices. Among these, five in the trimethyl-X-Y group also display a large variation in electronic band gaps that could make them useful for multisource energy harvesting. Ten likely plastic molecular crystals and ten likely plastic ionic molecular crystals were identified among the candidate systems by comparing the crystal structures of the candidate systems with close-packed crystal structures.

Our study has successfully identified a range of candidate ferroelectric molecular and molecular ionic crystals, including 16 that have been reported as ferroelectrics in the past. The screening criteria used were quite strict, and relaxing some of them, such as the size limitations on both molecules and unit cells, would have expanded the pool. The criteria were based on previously reported ferroelectric molecular and molecular ionic crystals. For this reason, crystal structures that differ significantly from the earlier reported ones could have been overlooked. Still, the identification of the boron cluster-based systems was unexpected, illustrating the potency of the CSD screening. In the design of novel ferroelectric plastic crystals, a good starting point is combining different globular molecular species, e.g., combinations of cations and anions. The various molecular species in the systems identified here and the corresponding crystal structures can serve as inspiration for such design.

In this study, we have not assessed whether the polarizations of the candidate ferroelectrics are switchable, which is a criterion for ferroelectricity. However, all of the candidate systems will necessarily have pyro- and piezoelectric properties as of their polar crystal symmetries. This study and the identified systems should stimulate further theoretical or experimental studies to assess their ferroelectric switchability and other characteristics such as the Curie temperatures and material stability.

■ ASSOCIATED CONTENT

Data Availability Statement

All the relaxed crystal structures used in this study can be accessed through the NOMAD database at https://dx.doi.org/10.17172/NOMAD/2023.06.12-1. All other data are available upon reasonable request. Scripts for computing globularity and Network properties are available in the Molcrys package.

Supporting Information

The Supporting Information is available free of charge at https://pubs.acs.org/doi/10.1021/acs.cgd.3c00713.

Description of the screening tools and criteria used for molecular geometries, including the evaluation of the globularity of molecules and the identification of extended linear segments (PDF)

■ AUTHOR INFORMATION

Corresponding Authors

Elin Dypvik Sødahl − *Department of Mechanical Engineering and Technology Management, Norwegian University of Life Sciences, 1432 Ås, Norway;* orcid.org/0000-0001-8877-9044; Email: elin.dypvik.sodahl@nmbu.no

Kristian Berland − *Department of Mechanical Engineering and Technology Management, Norwegian University of Life Sciences, 1432 Ås, Norway;* orcid.org/0000-0002-4655-1233; Email: kristian.berland@nmbu.no

Authors

Seyedmojtaba Seyedraoufi − *Department of Mechanical Engineering and Technology Management, Norwegian University of Life Sciences, 1432 Ås, Norway;* orcid.org/0000-0003-3800-0412

Carl Henrik Görbitz − *Department of Chemistry, University of Oslo, 0371 Oslo, Norway*

Complete contact information is available at: https://pubs.acs.org/10.1021/acs.cgd.3c00713

Notes

The authors declare no competing financial interest.

■ ACKNOWLEDGMENTS

The computations of this work were carried out on UNINETT Sigma2 high-performance computing resources (grant NN9650K). This work is supported by the Research Council of Norway as a part of the Young Research Talent project FOX (302362).

■ REFERENCES

(1) Vijayakanth, T.; Liptrot, D. J.; Gazit, E.; Boomishankar, R.; Bowen, C. R. Recent Advances in Organic and Organic−Inorganic Hybrid Materials for Piezoelectric Mechanical Energy Harvesting. *Adv. Funct. Mater.* **2022**, *32*, 2109492.

(2) Pan, Q.; Xiong, Y.-A.; Sha, T.-T.; You, Y.-M. Recent progress in the piezoelectricity of molecular ferroelectrics. *Mater. Chem. Front.* **2021**, *5*, 44−59.

(3) Tayi, A. S.; Kaeser, A.; Matsumoto, M.; Aida, T.; Stupp, S. I. Supramolecular ferroelectrics. *Nat. Chem.* **2015**, *7*, 281−294.

(4) Zhang, Y.; Di, F.; Li, P.; Xiong, R. Crown Ether Host-Guest Molecular Ferroelectrics. *Chem.—Eur. J.* **2022**, *28*, No. e202102990.

(5) Harada, J.; Shimojo, T.; Oyamaguchi, H.; Hasegawa, H.; Takahashi, Y.; Satomi, K.; Suzuki, Y.; Kawamata, J.; Inabe, T. Directionally tunable and mechanically deformable ferroelectric crystals from rotating polar globular ionic molecules. *Nat. Chem.* **2016**, *8*, 946−952.

(6) Deng, S.; Li, J.; Chen, X.; Hou, Y.; Chen, L. A novel ferroelectric based on quinuclidine derivatives. *Chin. Chem. Lett.* **2020**, *31*, 1686−1689.
(7) Lan, X.; Wang, X.; Zhang, D. X.; Mu, T.; Lan, X. Z. Cation and Anion Transfer in Quinuclidinium Hexafluorophosphate Plastic Crystal: Role of Constituent Ions and the Crystalline Structure. *J. Phys. Chem. C* **2021**, *125*, 21169−21178.
(8) Owczarek, M.; Hujsak, K. A.; Ferris, D. P.; Prokofjevs, A.; Majerz, I.; Szklarz, P.; Zhang, H.; Sarjeant, A. A.; Stern, C. L.; Jakubas, R.; Hong, S.; Dravid, V. P.; Stoddart, J. F. Flexible ferroelectric organic crystals. *Nat. Commun.* **2016**, *7*, 13108.
(9) Walker, J.; Scherrer, S.; Løndal, N. S.; Grande, T.; Einarsrud, M.-A. Electric field dependent polarization switching of tetramethylammonium bromotrichloroferrate(III) ferroelectric plastic crystals. *Appl. Phys. Lett.* **2020**, *116*, 242902.
(10) Hu, Y.; Gottfried, J. L.; Pesce-Rodriguez, R.; Wu, C.-C.; Walck, S. D.; Liu, Z.; Balakrishnan, S.; Broderick, S.; Guo, Z.; Zhang, Q.; An, L.; Adlakha, R.; Nouh, M.; Zhou, C.; Chung, P. W.; Ren, S. Releasing chemical energy in spatiallyprogrammed ferroelectrics. *Nat. Commun.* **2022**, *13*, 6959.
(11) Horiuchi, S.; Ishibashi, S. Hydrogen-Bonded Small-Molecular Crystals Yielding Strong Ferroelectric and Antiferroelectric Polarizations. *J. Phys. Soc. Jpn.* **2020**, *89*, 051009.
(12) Shi, P.-P.; Tang, Y.-Y.; Li, P.-F.; Liao, W.-Q.; Wang, Z.-X.; Ye, Q.; Xiong, R.-G. Symmetry breaking in molecular ferroelectrics. *Chem. Soc. Rev.* **2016**, *45*, 3811−3827.
(13) Sun, Z.; Yi, X.; Tao, K.; Ji, C.; Liu, X.; Li, L.; Han, S.; Zheng, A.; Hong, M.; Luo, J. A Molecular Ferroelectric Showing Room-Temperature Record-Fast Switching of Spontaneous Polarization. *Angew. Chem.* **2018**, *130*, 9981−9985.
(14) Gao, K.; Gu, M.; Qiu, X.; Ying, X. N.; Ye, H.-Y.; Zhang, Y.; Sun, J.; Meng, X.; Zhang, F. M.; Wu, D.; Cai, H.-L.; Wu, X. S. Above-room-temperature molecular ferroelectric and fast switchable dielectric of diisopropylammonium perchlorate. *J. Mater. Chem. C* **2014**, *2*, 9957−9963.
(15) Tang, Y.-Y.; Zhang, W.-Y.; Li, P.-F.; Ye, H.-Y.; You, Y.-M.; Xiong, R.-G. Ultrafast Polarization Switching in a Biaxial Molecular Ferroelectric Thin Film: [Hdabco]ClO_4. *J. Am. Chem. Soc.* **2016**, *138*, 15784−15789.
(16) Sødahl, E. D.; Walker, J.; Berland, K. Piezoelectric Response of Plastic Ionic Molecular Crystals: Role of Molecular Rotation. *Cryst. Growth Des.* **2023**, *23*, 729−740.
(17) You, Y.-M.; Tang, Y.-Y.; Li, P.-F.; Zhang, H.-Y.; Zhang, W.-Y.; Zhang, Y.; Ye, H.-Y.; Nakamura, T.; Xiong, R.-G. Quinuclidinium salt ferroelectric thin-film with duodecuple-rotational polarization-directions. *Nat. Commun.* **2017**, *8*, 14934.
(18) Xie, Y.; Ai, Y.; Zeng, Y.-L.; He, W.-H.; Huang, X.-Q.; Fu, D.-W.; Gao, J.-X.; Chen, X.-G.; Tang, Y.-Y. The Soft Molecular Polycrystalline Ferroelectric Realized by the Fluorination Effect. *J. Am. Chem. Soc.* **2020**, *142*, 12486−12492.
(19) Wang, B.; Ma, D.; Zhao, H.; Long, L.; Zheng, L. Room Temperature Lead-Free Multiaxial Inorganic−Organic Hybrid Ferroelectric. *Inorg. Chem.* **2019**, *58*, 13953−13959.
(20) Das, S.; Mondal, A.; Reddy, C. M. Harnessing molecular rotations in plastic crystals: a holistic view for crystal engineering of adaptive soft materials. *Chem. Soc. Rev.* **2020**, *49*, 8878−8896.
(21) Yang, C.-K.; Chen, W.-N.; Ding, Y.-T.; Wang, J.; Rao, Y.; Liao, W.-Q.; Xie, Y.; Zou, W.; Xiong, R.-G. Directional Intermolecular Interactions for Precise Molecular Design of a High- T_c Multiaxial Molecular Ferroelectric. *J. Am. Chem. Soc.* **2019**, *141*, 1781−1787.
(22) Harada, J. Plastic/ferroelectric molecular crystals: Ferroelectric performance in bulk polycrystalline forms. *APL Mater.* **2021**, *9*, 020901.
(23) Ai, Y.; Zeng, Y.-L.; He, W.-H.; Huang, X.-Q.; Tang, Y.-Y. Six-Fold Vertices in a Single-Component Organic Ferroelectric with Most Equivalent Polarization Directions. *J. Am. Chem. Soc.* **2020**, *142*, 13989−13995.
(24) Tang, Y.-Y.; Li, P.-F.; Zhang, W.-Y.; Ye, H.-Y.; You, Y.-M.; Xiong, R.-G. A Multiaxial Molecular Ferroelectric with Highest Curie Temperature and Fastest Polarization Switching. *J. Am. Chem. Soc.* **2017**, *139*, 13903−13908.
(25) Zhang, Y.; Song, X.-J.; Zhang, Z.-X.; Fu, D.-W.; Xiong, R.-G. Piezoelectric Energy Harvesting Based on Multiaxial Ferroelectrics by Precise Molecular Design. *Matter* **2020**, *2*, 697−710.
(26) Zafar, Z.; Zafar, A.; Guo, X.; Lin, Q.; Yu, Y. Raman evolution of order−disorder phase transition in multiaxial molecular ferroelectric thin film. *J. Raman Spectrosc.* **2019**, *50*, 1576−1583.
(27) Tang, Y.-Y.; Li, P.-F.; Liao, W.-Q.; Shi, P.-P.; You, Y.-M.; Xiong, R.-G. Multiaxial Molecular Ferroelectric Thin Films Bring Light to Practical Applications. *J. Am. Chem. Soc.* **2018**, *140*, 8051−8059.
(28) Zhang, H.-Y.; Tang, Y.-Y.; Shi, P.-P.; Xiong, R.-G. Toward the Targeted Design of Molecular Ferroelectrics: Modifying Molecular Symmetries and Homochirality. *Acc. Chem. Res.* **2019**, *52*, 1928−1938.
(29) Baudry, L.; Lukyanchuk, I.; Vinokur, V. M. Ferroelectric symmetry-protected multibit memory cell. *Sci. Rep.* **2017**, *7*, 42196.
(30) Timmermans, J. Plastic crystals: A historical review. *J. Phys. Chem. Solids* **1961**, *18*, 1−8.
(31) Ishida, H.; Iwachido, T.; Hayama, N.; Ikeda, R.; Hashimoto, M.; Nakamura, D. Structural Phase Transitions in Solid tert-Butylammonium Nitrate as Studied by Differential Thermal Analysis and ^{1}H-NMR. *Z. Naturforsch. A* **1989**, *44*, 71−74.
(32) Pringle, J. M. Recent progress in the development and use of organic ionic plastic crystal electrolytes. *Phys. Chem. Chem. Phys.* **2013**, *15*, 1339−1351.
(33) Wei, Z.-H.; Jiang, Z.-T.; Zhang, X.-X.; Li, M.-L.; Tang, Y.-Y.; Chen, X.-G.; Cai, H.; Xiong, R.-G. Rational Design of Ceramic-Like Molecular Ferroelectric by Quasi-Spherical Theory. *J. Am. Chem. Soc.* **2020**, *142*, 1995−2000.
(34) Mondal, A.; Bhattacharya, B.; Das, S.; Bhunia, S.; Chowdhury, R.; Dey, S.; Reddy, C. M. Metal-like Ductility in Organic Plastic Crystals: Role of Molecular Shape and Dihydrogen Bonding Interactions in Aminoboranes. *Angew. Chem., Int. Ed.* **2020**, *59*, 10971−10980.
(35) Saha, S.; Mishra, M. K.; Reddy, C. M.; Desiraju, G. R. From Molecules to Interactions to Crystal Engineering: Mechanical Properties of Organic Solids. *Acc. Chem. Res.* **2018**, *51*, 2957−2967.
(36) Olejniczak, A.; Anioła, M.; Szafrański, M.; Budzianowski, A.; Katrusiak, A. New Polar Phases of 1,4-Diazabicyclo[2.2.2]octane Perchlorate, An $NH^+ \cdots N$ Hydrogen-Bonded Ferroelectric. *Cryst. Growth Des.* **2013**, *13*, 2872−2879.
(37) Olejniczak, A.; Szafrański, M.; Katrusiak, A. Pressure−Temperature Phase Diagrams and Transition Mechanisms of Hybrid Organic−Inorganic NH··· N Bonded Ferroelectrics. *Cryst. Growth Des.* **2018**, *18*, 6488−6496.
(38) Harada, J.; Kawamura, Y.; Takahashi, Y.; Uemura, Y.; Hasegawa, T.; Taniguchi, H.; Maruyama, K. Plastic/Ferroelectric Crystals with Easily Switchable Polarization: Low-Voltage Operation, Unprecedentedly High Pyroelectric Performance, and Large Piezoelectric Effect in Polycrystalline Forms. *J. Am. Chem. Soc.* **2019**, *141*, 9349−9357.
(39) Cohen, R. E. Origin of ferroelectricity in perovskite oxides. *Nature* **1992**, *358*, 136−138.
(40) Ai, Y.; Wu, D.-J.; Yang, M.-J.; Wang, P.; He, W.-H.; Liao, W.-Q. Highest-Tc organic enantiomeric ferroelectrics obtained by F/H substitution. *Chem. Commun.* **2020**, *56*, 7033−7036.
(41) Tang, Y.-Y.; Xie, Y.; Ai, Y.; Liao, W.-Q.; Li, P.-F.; Nakamura, T.; Xiong, R.-G. Organic Ferroelectric Vortex−Antivortex Domain Structure. *J. Am. Chem. Soc.* **2020**, *142*, 21932−21937.
(42) Groom, C. R.; Bruno, I. J.; Lightfoot, M. P.; Ward, S. C. The Cambridge Structural Database. *Acta Crystallogr., Sect. B: Struct. Sci., Cryst. Eng. Mater.* **2016**, *72*, 171−179.
(43) Seyedraoufi, S.; Sødahl, E. D.; Görbitz, C. H.; Berland, K. Database mining and first-principles assessment of organic proton-transfer ferroelectrics. **2023**, arXiv:2306.00363.
(44) All structure and molecule figures are made using the software programs Mercury96 and VESTA.97

https://doi.org/10.1021/acs.cgd.3c00713
Cryst. Growth Des. 2023, 23, 8607−8619

(45) Berland, K.; Sødahl, E. D.; Seyedraoufi, S. Molcrys, 2023. https://gitlab.com/m7582/molcrys/.
(46) Hjorth Larsen, A.; Jørgen Mortensen, J.; Blomqvist, J.; Castelli, I. E.; Christensen, R.; Dułak, M.; Friis, J.; Groves, M. N.; Hammer, B.; Hargus, C.; Hermes, E. D.; Jennings, P. C.; Bjerre Jensen, P.; Kermode, J.; Kitchin, J. R.; Leonhard Kolsbjerg, E.; Kubal, J.; Kaasbjerg, K.; Lysgaard, S.; Bergmann Maronsson, J.; Maxson, T.; Olsen, T.; Pastewka, L.; Peterson, A.; Rostgaard, C.; Schiøtz, J.; Schütt, O.; Strange, M.; Thygesen, K. S.; Vegge, T.; Vilhelmsen, L.; Walter, M.; Zeng, Z.; Jacobsen, K. W. The atomic simulation environment—a python library for working with atoms. *J. Condens. Matter Phys.* **2017**, *29*, 273002.
(47) Hagberg, A.; Swart, P.; Chult, D. S. *Exploring Network Structure, Dynamics, and Function Using Networkx*, 2008.
(48) André, D.; Dworkin, A.; Szwarc, H.; Céolin, R.; Agafonov, V.; Fabre, C.; Rassat, A.; Straver, L.; Bernier, P.; Zahab, A. Molecular packing of fullerene C_{60} at room temperature. *Mol. Phys.* **1992**, *76*, 1311−1317.
(49) Jenkins, T. E.; Lewis, J. A Raman study of adamantane (C10H16), diamantane (C14H20) and triamantane (C18H24) between 10 K and room temperatures. *Spectrochim. Acta, Part A* **1980**, *36*, 259−264.
(50) Szewczyk, D.; Jeżowski, A.; Krivchikov, A. I.; Tamarit, J. L. Influence of thermal treatment on thermal properties of adamantane derivatives. *Low Temp. Phys.* **2015**, *41*, 469−472.
(51) Bruno, I. J.; Cole, J. C.; Edgington, P. R.; Kessler, M.; Macrae, C. F.; McCabe, P.; Pearson, J.; Taylor, R. New software for searching the Cambridge Structural Database and visualizing crystal structures. *Acta Crystallogr., Sect. B: Struct. Sci.* **2002**, *58*, 389−397.
(52) Kresse, G.; Hafner, J. Ab initio molecular-dynamics simulation of the liquid-metal−amorphous-semiconductor transition in germanium. *Phys. Rev. B: Condens. Matter Mater. Phys.* **1994**, *49*, 14251−14269.
(53) Kresse, G.; Hafner, J. Ab initio molecular dynamics for liquid metals. *Phys. Rev. B: Condens. Matter Mater. Phys.* **1993**, *47*, 558−561.
(54) Kresse, G.; Furthmüller, J. Efficiency of ab-initio total energy calculations for metals and semiconductors using a plane-wave basis set. *Comput. Mater. Sci.* **1996**, *6*, 15−50.
(55) Kresse, G.; Furthmüller, J. Efficient iterative schemes for *ab initio* total-energy calculations using a plane-wave basis set. *Phys. Rev. B: Condens. Matter Mater. Phys.* **1996**, *54*, 11169−11186.
(56) Blöchl, P. E. Projector augmented-wave method. *Phys. Rev. B: Condens. Matter Mater. Phys.* **1994**, *50*, 17953−17979.
(57) Kresse, G.; Joubert, D. From ultrasoft pseudopotentials to the projector augmented-wave method. *Phys. Rev. B: Condens. Matter Mater. Phys.* **1999**, *59*, 1758−1775.
(58) Resta, R. Macroscopic polarization in crystalline dielectrics: the geometric phase approach. *Rev. Mod. Phys.* **1994**, *66*, 899−915.
(59) Baroni, S.; Resta, R. *Ab initio* calculation of the macroscopic dielectric constant in silicon. *Phys. Rev. B: Condens. Matter Mater. Phys.* **1986**, *33*, 7017−7021.
(60) Berland, K.; Hyldgaard, P. Exchange functional that tests the robustness of the plasmon description of the van der Waals density functional. *Phys. Rev. B: Condens. Matter Mater. Phys.* **2014**, *89*, 035412.
(61) Harada, J.; Yoneyama, N.; Yokokura, S.; Takahashi, Y.; Miura, A.; Kitamura, N.; Inabe, T. Ferroelectricity and piezoelectricity in free-standing polycrystalline films of plastic crystals. *J. Am. Chem. Soc.* **2018**, *140*, 346−354.
(62) Chen, X.-G.; Song, X.-J.; Zhang, Z.-X.; Zhang, H.-Y.; Pan, Q.; Yao, J.; You, Y.-M.; Xiong, R.-G. Confinement-Driven Ferroelectricity in a Two-Dimensional Hybrid Lead Iodide Perovskite. *J. Am. Chem. Soc.* **2020**, *142*, 10212−10218.
(63) Szafrański, M.; Katrusiak, A.; McIntyre, G. J. Ferroelectric Order of Parallel Bistable Hydrogen Bonds. *Phys. Rev. Lett.* **2002**, *89*, 215507.
(64) Tang, Y.-Y.; Zhang, W.-Y.; Li, P.-F.; Ye, H.-Y.; You, Y.-M.; Xiong, R.-G. Ultrafast polarization switching in a biaxial molecular ferroelectric thin film: [Hdabco]ClO4. *J. Am. Chem. Soc.* **2016**, *138*, 15784−15789.
(65) Budzianowski, A.; Katrusiak, A. Anomalous Protonic-Glass Evolution from Ordered Phase in NH ··· N Hydrogen-Bonded DabcoHBF4 Ferroelectric. *J. Phys. Chem. B* **2008**, *112*, 16619−16625.
(66) Ye, H.-Y.; Tang, Y.-Y.; Li, P.-F.; Liao, W.-Q.; Gao, J.-X.; Hua, X.-N.; Cai, H.; Shi, P.-P.; You, Y.-M.; Xiong, R.-G. Metal-free three-dimensional perovskite ferroelectrics. *Science* **2018**, *361*, 151−155.
(67) Siczek, M.; Lis, T. (*R*)-(−)-3-Hydroxyquinuclidinium chloride. *Acta Crystallogr., Sect. E: Struct. Rep. Online* **2008**, *64*, 842.
(68) Li, P.-F.; Tang, Y.-Y.; Wang, Z.-X.; Ye, H.-Y.; You, Y.-M.; Xiong, R.-G. Anomalously rotary polarization discovered in homochiral organic ferroelectrics. *Nat. Commun.* **2016**, *7*, 13635.
(69) Li, P.-F.; Liao, W.-Q.; Tang, Y.-Y.; Qiao, W.; Zhao, D.; Ai, Y.; Yao, Y.-F.; Xiong, R.-G. Organic enantiomeric high- T_c ferroelectrics. *Proc. Natl. Acad. Sci. U.S.A.* **2019**, *116*, 5878−5885.
(70) Zhang, Y.; Hopkins, M. A.; Liptrot, D. J.; Khanbareh, H.; Groen, P.; Zhou, X.; Zhang, D.; Bao, Y.; Zhou, K.; Bowen, C. R.; Carbery, D. R. Harnessing Plasticity in an Amine-Borane as a Piezoelectric and Pyroelectric Flexible Film. *Angew. Chem., Int. Ed.* **2020**, *59*, 7808−7812.
(71) Shi, P.-P.; Ye, Q.; Li, Q.; Wang, H.-T.; Fu, D.-W.; Zhang, Y.; Xiong, R.-G. Novel Phase-Transition Materials Coupled with Switchable Dielectric, Magnetic, and Optical Properties: [(CH3)4P][FeCl4] and [(CH3)4P][FeBr4]. *Chem. Mater.* **2014**, *26*, 6042−6049.
(72) Szafrański, M. Strong negative thermal expansion and relaxor ferroelectricity driven by supramolecular patterns. *J. Mater. Chem. C* **2013**, *1*, 7904.
(73) Olejniczak, A.; Katrusiak, A.; Szafrański, M. Ten polymorphs of nh+ ··· n hydrogen-bonded 1,4-diazabicyclo[2.2.2]octane complexes: Supramolecular origin of giant anisotropic dielectric response in polymorph V. *Cryst. Growth Des.* **2010**, *10*, 3537−3546.
(74) Szafrański, M. Temperature-induced displacement of the proton site in strong f−h−f hydrogen bond and mechanism of phase transition in 1,4 diazabicyclo[2.2.2]octane dihydrogen difluoride. *Chem. Phys. Lett.* **2008**, *457*, 110.
(75) Bläsing, K.; Labbow, R.; Schulz, A.; Villinger, A. Silylated sulfuric acid: Preparation of a tris(trimethylsilyl)oxosulfonium [(me3si-o)3so]+ salt. *Angew. Chem., Int. Ed.* **2021**, *60*, 13798−13802.
(76) Krukau, A. V.; Vydrov, O. A.; Izmaylov, A. F.; Scuseria, G. E. Influence of the exchange screening parameter on the performance of screened hybrid functionals. *J. Chem. Phys.* **2006**, *125*, 224106.
(77) Maglione, M.; Philippot, G.; Levasseur, D.; Payan, S.; Aymonier, C.; Elissalde, C. Defect chemistry in ferroelectric perovskites: long standing issues and recent advances. *Dalton Trans.* **2015**, *44*, 13411−13418.
(78) Damjanovic, D. Ferroelectric, dielectric and piezoelectric properties of ferroelectric thin films and ceramics. *Rep. Prog. Phys.* **1998**, *61*, 1267−1324.
(79) Fu, D.-W.; Gao, J.-X.; He, W.-H.; Huang, X.-Q.; Liu, Y.-H.; Ai, Y. High-Tc Enantiomeric Ferroelectrics Based on Homochiral Dabco-derivatives (Dabco = 1,4-Diazabicyclo[2.2.2]octane). *Angew. Chem., Int. Ed.* **2020**, *59*, 17477−17481.
(80) Li, J.-Y.; Xu, Q.-L.; Ye, S.-Y.; Tong, L.; Chen, X.; Chen, L.-Z. A multiaxial molecular ferroelectric with record high T_c designed by intermolecular interaction modulation. *Chem. Commun.* **2021**, *57*, 943−946.
(81) Yoneya, M.; Harada, J. Molecular Dynamics Simulation Study of the Plastic/Ferroelectric Crystal Quinuclidinium Perrhenate. *J. Phys. Chem. C* **2020**, *124*, 2171−2177.
(82) Lee, J.; Seol, W.; Anoop, G.; Samanta, S.; Unithrattil, S.; Ahn, D.; Kim, W.; Jung, G.; Jo, J. Stabilization of Ferroelectric Phase in Highly Oriented Quinuclidinium Perrhenate (HQReO4) Thin Films. *Materials* **2021**, *14*, 2126.
(83) Li, J. L.; Yang, G. W. Iron Endohedral-Doped Boron Fullerene: A Potential Single Molecular Device with Tunable Electronic and Magnetic Properties. *J. Phys. Chem. C* **2009**, *113*, 18292−18295.

https://doi.org/10.1021/acs.cgd.3c00713
Cryst. Growth Des. 2023, 23, 8607−8619

(84) Ma, L.; He, H.; Yang, B.-F.; Zhang, Q.; Yang, G.-Y. [Pb(en)0.5][B5O8(OH)]: A New Bilayered Organic−Inorganic Hybrid Lead Borate Built by B5O8(OH) Cluster Units. *J. Cluster Sci.* **2015**, *26*, 1495−1502.
(85) Zhao, D.; He, X.; Li, M.; Wang, B.; Guo, C.; Rong, C.; Chattaraj, P. K.; Liu, S. Density functional theory studies of boron clusters with exotic properties in bonding, aromaticity and reactivity. *Phys. Chem. Chem. Phys.* **2021**, *23*, 24118−24124.
(86) Barba-Bon, A.; Salluce, G.; Lostalé-Seijo, I.; Assaf, K. I.; Hennig, A.; Montenegro, J.; Nau, W. M. Boron clusters as broadband membrane carriers. *Nature* **2022**, *603*, 637−642.
(87) Li, D.; Zhao, X.-M.; Zhao, H.-X.; Long, L.-S.; Zheng, L.-S. Coexistence of Magnetic-Optic-Electric Triple Switching and Thermal Energy Storage in a Multifunctional Plastic Crystal of Trimethylchloromethyl Ammonium Tetrachloroferrate(III). *Inorg. Chem.* **2019**, *58*, 655−662.
(88) Even, J.; Carignano, M.; Katan, C. Molecular disorder and translation/rotation coupling in the plastic crystal phase of hybrid perovskites. *Nanoscale* **2016**, *8*, 6222−6236.
(89) Létoublon, A.; Paofai, S.; Rufflé, B.; Bourges, P.; Hehlen, B.; Michel, T.; Ecolivet, C.; Durand, O.; Cordier, S.; Katan, C.; Even, J. Elastic Constants, Optical Phonons, and Molecular Relaxations in the High Temperature Plastic Phase of the $CH_3NH_3PbBr_3$ Hybrid Perovskite. *J. Phys. Chem. Lett.* **2016**, *7*, 3776−3784.
(90) Shang, Y.; Sun, L.-y.; Ye, Z.-m.; Chen, S.-l.; Zhang, W.-x.; Chen, X.-m. Phase transition and thermal expansion of molecular perovskite energetic crystal (C6N2H14)(NH4)(ClO4)3 (DAP-4). *FirePhysChem* **2022**, *2*, 221−225.
(91) Staveley, L. A. K. Phase transitions in plastic crystals. *Annu. Rev. Phys. Chem.* **1962**, *13*, 351−368.
(92) Li, P.-F.; Tang, Y.-Y.; Liao, W.-Q.; Ye, H.-Y.; Zhang, Y.; Fu, D.-W.; You, Y.-M.; Xiong, R.-G. A semiconducting molecular ferroelectric with a bandgap much lower than that of BiFeO3. *NPG Asia Mater.* **2017**, *9*, No. e342.
(93) Bai, Y.; Jantunen, H.; Juuti, J. Energy Harvesting Research: The Road from Single Source to Multisource. *Adv. Mater.* **2018**, *30*, 1707271.
(94) Liu, H.-Y.; Zhang, H.-Y.; Chen, X.-G.; Xiong, R.-G. Molecular Design Principles for Ferroelectrics: Ferroelectrochemistry. *J. Am. Chem. Soc.* **2020**, *142*, 15205−15218.
(95) Lin, J.-H.; Lou, J.-R.; Ye, L.-K.; Hu, B.-L.; Zhuge, P.-C.; Fu, D.-W.; Su, C.-Y.; Zhang, Y. Halogen Engineering To Realize Regulable Multipolar Axes, Nonlinear Optical Response, and Piezoelectricity in Plastic Ferroelectrics. *Inorg. Chem.* **2023**, *62*, 2870−2876.

https://doi.org/10.1021/acs.cgd.3c00713
Cryst. Growth Des. 2023, 23, 8607−8619